RESEARCH REVIEW JOURNALS
Volume-05
Issue-05
May-2020

ISSN: 2455-3085 (Online)
RESEARCH REVIEW International Journal of Multidisciplinary
www.rrjournals.com[Peer Reviewed Journal]
DOI: https://doi.org/10.31305/rrijm.2020.v05.i05.004

Sonochemical synthesis of Nickel doped ZnO Nanostructures for Environmental Remediation

[1]M. Sudha, [2]S. Surendhiran, [2]P. Manoj Kumar and [3*]A. Balamurugan

[1]*Department of Physics, Government Arts College, Udhagamandalam – 643002, Tamilnadu (India)*
[2]*Centre for Nanoscience and Technology, KS Rangasamy College of Technology, Tiruchengode – 637 215, Tamilnadu (India)*
[3]*Department of Physics, Government Arts and Science College, Avinashi – 641654, Tamilnadu (India)*

ARTICLE DETAILS

Article History
Published Online: 15 May 2020

Keywords
Ni doped ZnO nanostructures; Sonochemical method; Rhodamine B dye; photocatalytic activity.

[*]Corresponding Author
Email: bala.snr[at]gmail.com

ABSTRACT

Zinc Oxide (ZnO) nanoparticles and Nickel doped ZnO nanostructures with 2.5, 5 and 7.5 wt.% of Ni concentrations were synthesized by simple sonochemical method. The prepared Ni doped ZnO photocatalysts were characterized by X-ray diffraction (XRD), field emission scanning electron microscopy (FESEM), and Fourier transform infrared (FTIR) and UV–vis spectrophotometry. The obtained XRD and FESEM results confirmed the well dispersion of Ni nanoparticles with agglomeration with ZnO. The optical band gap value was calculated as 3.29, 3.21 and 3.18 eV from UV-Vis spectra of 2.5, 5 and 7.5 wt. % respectively. The photocatalytic activities were evaluated for sun light driven degradation of an aqueous Rhodamine B dye (RB) solution. The results of the photocatalytic degradation of Rhodamine B dye in aqueous solutions under the sun light showed that 7.5 wt. % of Ni/ZnO exhibited higher photocatalytic activity (93.3%) than the low Ni concentration doped ZnO (91.23 and 92.38 %) nanostructures.

1. Introduction

In current years, dyeing industrial pollution found more in the environment specially air and water poses serious health dangers to the human life [1, 2]. Therefore, the traits of the low cost technique to manage water air pollution think about pinnacle priority in cost effective research. Zinc Oxide is one of the most studied metal oxide substances due to the fact of its vast applications, such as photocatalysts, electrochemical and bio sensors, and organic applications [3-6]. To enhance the performances of pure ZnO, hybridization with metals (such as Ni) has considerably been employed. ZnO nanostructures are geared up with the useful resource of hydrothermal, solvothermal, electro deposition, and physical deposition methods [6-10] but an appropriate method for preparing ZnO at low processing cost, working at ambient temperature, smaller dimension vary and better belongings are a venture for researchers.

It reveals higher quantum effectively and photocatalytic endeavor than TiO_2 in high quality cases [11]. Hence, the photocatalytic recreation of ZnO has to be higher than the other elements by means of capacity of employing a range of strategies. One of the necessary strategies in improving the photocatalytic houses is doping the metal oxides which eventually effects in the version of surface vicinity and the incorporation of dopant ions generate lattice defects and modify bandgap power and it's considered optical response. Consequently, doping of transition metals, noble metals and non-metal is a very expedient way to enhance the photocatalytic activity [12-14].The crystal structure and surface morphologies play an eminent role in photocatalytic things to do of metal oxides. The doping with a transition metallic ion increases the surface defects. This can possibly shift the absorption in the direction of visible location (Red shift) [15-20]. The enhancement in optical absorption in surface defects with the aid of doping with Ni ion make us proceed in study of photocatalytic property in undoped (already reported) and doped ZnO nanoparticles.

To boost up the ZnO's photocatalytic activity, we doped Ni with ZnO nanostructures and photocatalytic degradation activity of Rhodamine B dye.

2. Experimental details

The Nickel (Ni) doped Zinc Oxide (ZnO) nanostructures have been synthesized by a chemical route such sonication method. The Chemicals used in our synthesis process are as follows: All the reagents were in analytical grade (AR) purity.

1. Zinc Nitrate (Zn $(NO_3)_2.6H_2O$)
2. Nickel Nitrate (Ni $(NO_3)_2.6H_2O$)
3. Sodium hydroxide (NaOH)
4. Distilled water (H_2O),)

2.1. Preparation of Ni doped ZnO nanostructures

An aqueous solution of Zinc nitrate (1M, 100 mL) and desired wt. % of Nickel nitrate in 100 mL was kept in sonication chamber with 40Hz power of ultrasonic wave irradiation. The Sonicator equipment setting parameters were fixed for 5 sec of irradiation and 5 sec for rest; during the rest time, the NaOH (1M, 100 mL) solution was added to adjust the pH value. After the pH value reached to 10, the solution was allowed to dry at 80°C for 6 hours and for calcination process at 400° C.

2.2. Characterization Techniques

Characterization Techniques such as X-Ray Diffraction (XRD), UV-Visible spectroscopy (UV-Vis), FESEM-coupled with EDX, particle size analyzer (PSA) were used to characterize the prepared Ni doped ZnO nanostructures.

To perceive the structural identification and the common crystallite dimension of the organized Ni doped ZnO nanostructures used to be used with the aid of X-ray diffractometer (X'Pert PRO; PANalytical, the Netherlands) CuKa radiation (λ = 1.5406 Å) used to be as a source to analyses the organized ZnO nanostructures at the 2θ from 10° to 80° with 2θ step of 0.02°. The UV absorption spectra of Ni doped ZnO nanostructures were recorded using UV–visible (UV–Vis) Spectrophotometer (Cary 8454; Agilent, Singapore) operated from the a180–800 nm spectral regions at a step measurement of 5 Å. The dispersed ZnO nanostructure (0.1 mg of Ni doped ZnO nanostructures used to be dispersed in 5 ml double deionized water and sonicated for three minutes for uniform dispersion) was taken in a cuvette. The particle size distribution and average particle size of the Ni doped ZnO nanostructures had been carried out with a submicrometre particle measurement analyzer (Nanophox; Sympatec, Zellerfeld, Germany) the use of dynamic light-scattering (DLS) technique. Field Emission Scanning electron microscope (FE- SEM; JSM-6790 LS; JEOL, forty Japan) was once used to analyze the surface morphology of the prepared Ni doped ZnO nanostructures.

2.3 Photocatalytic degradation of Rhodamine B dye

The photocatalytic degradation of Rhodamine B dye in the existence of Ni doped ZnO nanoparticles beneath sun light irradiation were once analyzed as follows. Briefly, a 100 mg of organized ZnO nanoparticles had been introduced into a 100 ml of aqueous Rhodamine B solution (50 mg/L) and stirred for 10 min to get clear suspension. Then appropriate volume of the supernatant Rhodamine B answer used to be taken with 15 minutes time interval to understand the awareness of Rhodamine B the use of UV-Vis spectrophotometer via the usage of absorption capability. Dye degradation successfully of ZnO nanoparticles beneath considered mild was as soon as determined the usage of the below relation.

Dye degradation efficiency $\eta = (1- C/C_0)$

Dye degradation efficiency where C and C_0 are final and initial concentration of Rhodamine B dye solution

3. Result and Discussion

3.1 XRD analysis

The XRD patterns of Ni-doped ZnO nanostructures at various amount of Ni content are shown in Fig.1 (i.e., a, b and c respectively for 2.5, 5 and 7.5 wt. % of Ni). The XRD records suggest that all the Ni-doped ZnO nanostructures having crystalline nature. The spectra for Ni doped ZnO nanostructures exhibit the broaden peaks at the positions of 36.87, 42.8, 62.18 and 74.53° having miller indices in where most intense peak found at (200) which are in right agreement with the well-known JCPDS file no. 75-0273 for Ni: ZnO [21 - 22]. It can be listed as the cubical structure of Ni doped ZnO with Fm3m (225) and some different unidentified diffraction peaks additionally seems it can also be without problems avoidable contents from environment.

It has been discovered that the diffraction peak alongside (200) increases with the nickel doping and then start growing with expand in the Ni concentration. Further, it is located that the peak intensities show off dramatic adjustments for all the corresponding planes with the insertion of Ni dopant and related to the degeneration of crystallinity. We have carried a relative analysis of crystallite dimension (D) of Ni doped ZnO nanostructures by means of Debye–Scherrer formula [23-25].

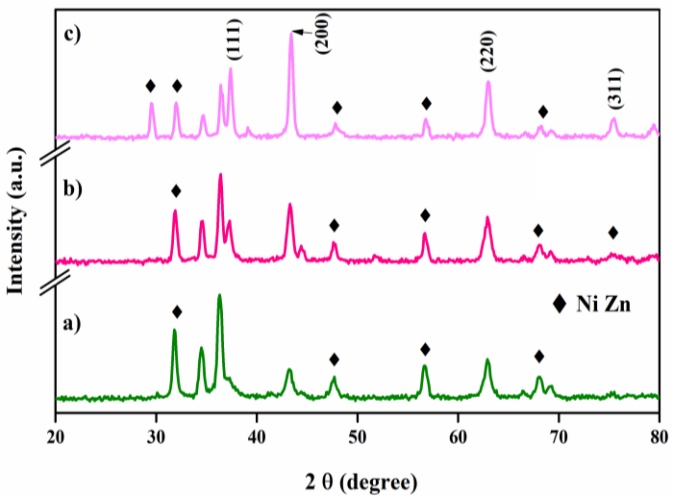

Fig. 1 shows XRD pattern of Ni doped ZnO nanostructures whereas a, b and c respectively for 2.5, 5 and 7.5 wt. % and Ni doped ZnO.

The common crystallite size (D) of samples have been determined the use of full width at half of most (FWHM) of the most extreme diffraction peak (101) thru the Debye–Scherrer components which is given below

$D= K\lambda/(\beta \cos \theta)$

Where D is crystallite size, θ is glancing factor (k = 0.9) and β is full width at half maxima (FWHM) of the peak. Using above equation we have decided crystallite dimension (D) for 2.5, 5 and 7.5 wt. % of Ni doping with ZnO nanostructures.

The average crystallite sizes (D) have been calculated using the Debye–Scherrer formulation as given above which are lying in the range of 15.6, 16.9 and 17.4 nm for 2.5, 5 and 7.5 wt. % Ni-doped ZnO nanostructures respectively. The average crystalline sizes were gradually increased while Ni concentration increased in ZnO doping mechanism [26-27].

3.2 Surface morphology

The surface morphology of the Ni doped ZnO nanostructures had been captured and discussed thru Field Emission Scanning electron microscopy (FESEM) and shown in fig. 2 (a, b and c respectively for 2.5, 5 and 7.5 wt. %). It was once located to be spherical in nature as proven in Fig. 2 (a) for 2.5 wt. % Ni doped ZnO nanostructures. Afterwards, the morphology have been started to agglomerate with nearest particles for 5 and 7.5 wt. % Ni doped ZnO nanostructures fig 2 (b & c).

X-Ray florescence (XRF) spectral evaluation has been carried out to confirm the chemical composition of the sample. Table. 1 shows the EDX spectra of Ni (2.5, 5 and 7.5 wt. %) doped ZnO which confirm that as organized nanostructures include solely Zn, O and Ni ions phase in the sample. These effects are effectively agreed with our XRD statistics and no different impurity phases have been located within Ni doped ZnO nanostructures [28-30].

3.3 FTIR analysis

Fig. 3 indicates the FTIR spectra of all samples and cited in vary of 400 to 4000 cm^{-1}. Fig. 3 presents the shift in the vibration frequencies of ZnO nanostructures ranging from 500 cm^{-1} to 1000 cm^{-1} due to the incorporation of Ni ions into the ZnO Wurtzite lattice and a strong absorption band lies in the range 400 cm^{-1} to 500 cm^{-1} which are ZnO stretching frequency (v). In addition, the spectra also suggests absorption peak parallel to O–H stretching vibration of the water molecule, an O−C−O stretching mode, (C=O) symmetric stretching vibration, Ni–O and Zn– O stretching mode corresponding to their vibrational frequencies [31-33]. These results show that Ni^{2+} ions have been nicely doped into ZnO lattice sites and additionally affirm the wurtzite shape of samples at room temperature.

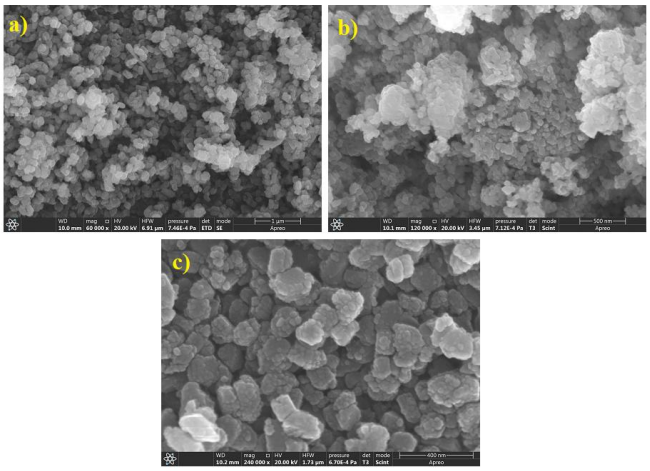

Fig. 2 shows FESEM image of Ni doped ZnO nanoparticles (a, b and c respectively for 2.5, 5 and 7.5 wt. % of Ni)

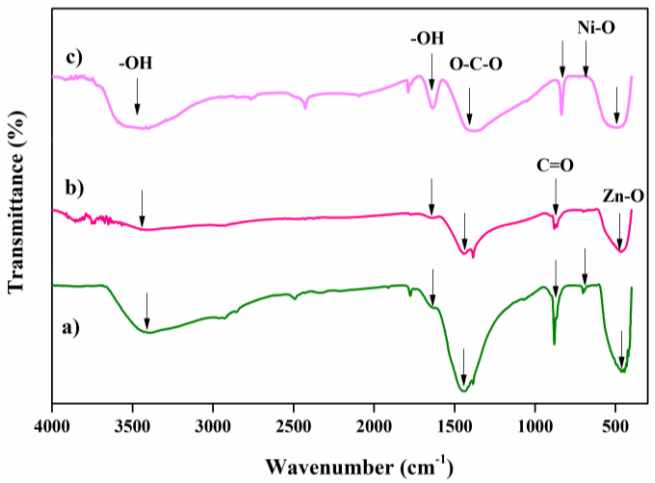

Fig. 3 shows FTIR pattern of Ni doped ZnO nanoparticles (a, b and c respectively for 2.5, 5 and 7.5 wt. % of Ni)

Table 1. XRF analysis of Ni doped ZnO nanostructures

S. No	Sample	Elements	Atomic concentrations (%)
1	2.5 wt. % Ni: ZnO	O	47.1
		Zn	50.4
		Ni	2.5
2	5.0 wt. % Ni: ZnO	O	46.9
		Zn	48.1
		Ni	5.0
3	7.5 wt. % Ni: ZnO	O	47.9
		Zn	44.6
		Ni	7.5

3.4 Particle size analysis

The average particle diameter (d_{50}) of the prepared Ni doped ZnO nanostructures have been degrees around 40 nm to 60 nm and actual values of average particle diameter measurement is given in fig. 4 (a, b and c respectively for 2.5, 5 and 7.5 wt. % Ni doped ZnO nanostructures). Since the size of the nanoparticles is most necessary ruling property for optical and electrical properties of the nanostructures, in a similar way for all different applications in accordance to quantum confinement effect. The average particle diameter distribution of 2.5, 5 and 7.5 wt. % Ni doped ZnO nanostructure are 44.5, 55.4 and 59.6 nm respectively. The sizes of the nanostructures are step by step reduced according to when Ni doping percentage amplifies in ZnO. The above results clearly indicate that the Ni doping with ZnO play a dominant role in measurement of the preparing nanostructures [35-37].

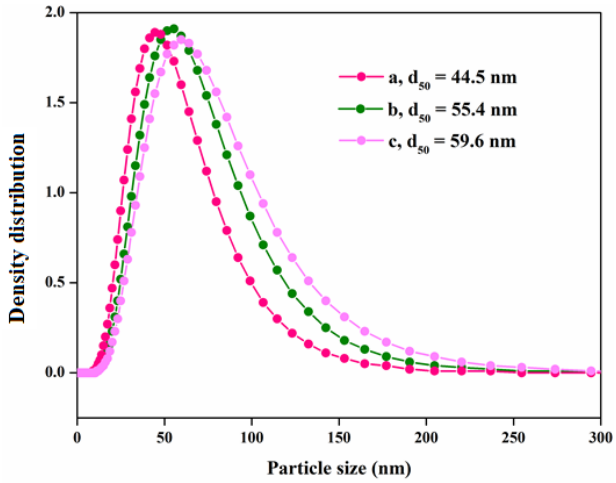

Fig. 4 shows particle diameter distribution curve of Ni doped ZnO nanostructures (a, b and c respectively for 2.5, 5 and 7.5 wt. % of Ni)

3.5 UV-Vis analysis

The UV absorption spectra of Ni doped ZnO nanostructures have been recorded in the range 200–800 nm. UV-vis spectra of Ni doped ZnO nanostructures showed an extensive deviation in absorption depth at the blue region (lower wavelength region) with expand in Ni doping concentration which is without a doubt seen in Fig 5. The large difference in the absorption intensity of Ni doped nanostructures suggests that Ni doped ZnO absorbs more visible light and so can act as a better photocatalyst underneath visible light irradiation. It is assumed that superior optical recreation is due to make bigger in surface imperfections due to doping in ZnO nanostructures [31, 33, and 38].

An enlargement in absorption intensity in blue region is attributed to extra pronounce doping of ZnO nanostructures with Ni ions. Doping of Ni with ZnO provides defect locations in the neighborhood of valence band and reduces the fantastic band gap. When UV-vis light is passed through prepared nanostructures the electron–hole pair is generated inside the fine band gap. It's capacity that the electron waft takes location from defect valence state to defect conduction state. This transition requires much lower energy than band hole of ZnO.

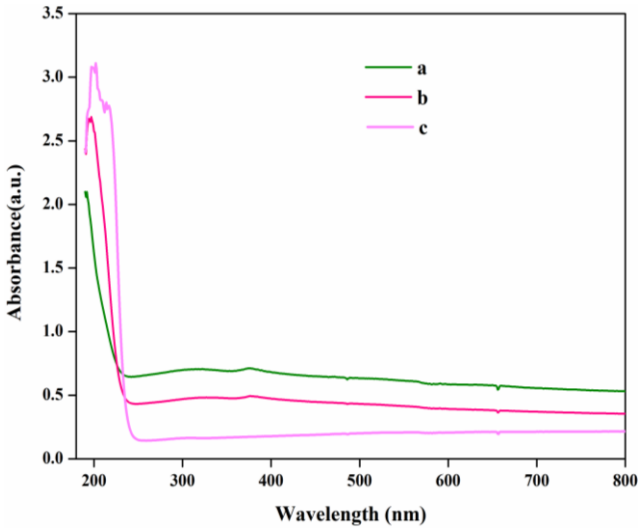

Fig. 5 shows UV-vis spectra of Ni doped ZnO nanostructures (a, b and c for 2.5, 5 and 7.5 wt. % of Ni)

The optical band gap energies of Ni doped ZnO nanostructures had been determined the usage of the Tauc relationship as given below [39-40]:

αhv=A((hv- Eg))^n

Where α is the absorption coefficient (α = 2.303A/t, where A is absorbance and t is thickness of the cuvette) and h, v and Eg are Planck's constant, photon frequency and optical band gap energy, respectively. The exponent (n) have the values 1/2, 3/2, 2 and 3 equivalent to the allowed direct, forbidden direct, allowed indirect and forbidden indirect transitions respectively.

The optical band gap was once various from 3.29, 3.21 and 3.18 eV for exclusive concentrations of Ni doped ZnO nanostructures. The markdown in the bandgap with the Ni concentration may want to be regarded as the introduction of Ni states in the pinnacle of valence band of ZnO nanostructures. These results also agreed with the suggested data (earlier reports).

3.6 Photocatalytic activity of Ni doped ZnO nanostructures

A major chunk of pollutants in contaminated water is from synthetic textile dyes and industrial dyes [41-42]. Rhodamine B dye is one of basically used dyes in the cloth industries consequently it is appreciably studied as a typical water pollutant and having probabilities to make health hazardless for human being. The degradation of Rhodamine B in the presence of organized ZnO nanostructures under solar light irradiation used to be studied for the length of 90 mins. Fig. 6 (a) (b) and (c) suggests the time constructed UV-Vis absorption spectrum of Rhodamine B dye in presence of 2.5, 5 and 7.5 wt. % of Ni doped ZnO nanostructures, respectively underneath the Sun light irradiation. It is mentioned that UV absorption of Rhodamine B dye at 554 nm falls rapidly with growing period which published that Ni doped ZnO nanostructures can easily oxidize the Rhodamine B dye underneath solar light illumination. Moreover, it is genuinely suggests that the photocatalytic assignment of 7.5 wt. % of Ni doped ZnO is substantially higher than that 2.5 and 5 wt. % Ni doped. The photocatalytic degradation effectively of 2.5, 5 and 7.5 wt. % of Ni doped ZnO nanostructures for the length of seventy five mins on Rhodamine B dye degradation are 91.23, 92.38 and 93.32 %, respectively.

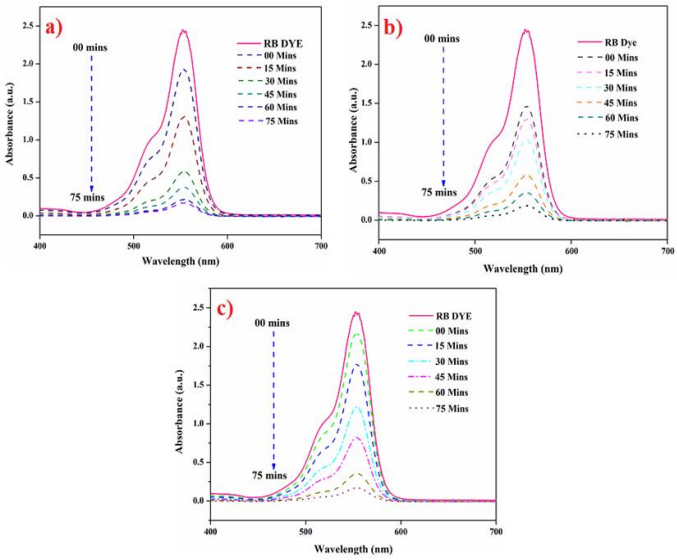

Fig. 6 shows photocatalytic degradation of Rhodamine B using Ni doped ZnO nanostructures whereas a, b and c for 2.5, 5 and 7.5 wt. % of Ni

In the visible light place the 5 wt. % Ni doped ZnO nanostructures degraded the Rhodamine B dye quicker than the 2.5 and 7.5 wt. % Ni doped ZnO nanostructures. The motive is being extended in surface defects on account of doping leading to improved absorption in the visible region. Once the above samples are irradiated to visible light (sun light), electron hole pair is generated. The electron so generated disrupts the conjugation in the dye and for that reason the decomposition of dye and the hole so generated creates OH from water which again leads to degradation of dye. The plot of absorption vs. wavelength at a range of instances for the photo degradation of Rhodamine B dye is represented in Fig. 6. It is seen in sketch that Ni doped ZnO degrades the 50% of dye in simply 15 minutes as in contrast to 2.5 wt. % of Ni doped ZnO which takes almost 30 minutes to degrade 50% of dye. ZnO nanostructures with the aid of doping can be used as workable photo catalytic retailers for degradation of dyes and different harmful organic compounds [43 -45].

3.7 Antibacterial activity of Ni doped ZnO nanostructures

The antibacterial activity of the Ni doped ZnO nanostructures were shown in Fig.7 (a, b, c, d, e & f). The maximum inhibitory concentration (30 mg/ml) shows zone of inhibition 20, 24 and 27 mm and zone of inhibition for lower concentration of nanostructures (15 mg/ml) 16, 17 and 20 mm against *S.aureus* respectively for 2.5, 5 and 7.5 wt. % Ni doped ZnO nanostructures. The maximum inhibitory concentration (30 mg/ml) shows zone of inhibition 13, 12 and 14 mm and zone of inhibition for lower concentration of nanostructures (15 mg/ml) 11, 13 and 12 mm against *E.coli* respectively for 2.5, 5 and 7.5 wt. % Ni doped ZnO nanostructures. The Commercial antibiotic Tetracycline (30 mg) reveals zone of inhibition 28, 26 and 26 mm against *S.aureus* and 24, 23 and 24 against *E.coli* for 2.5, 5 and 7.5 wt. % Ni doped ZnO nanostructures respectively. The Antibacterial activity of the 7.5 wt. % doped ZnO nanostructures are high due to large surface area to volume ratio. Also smallest particle size leads to cell death via penetrate cell wall and altered the cell membrane, cytoplasmic components. In addition, release of Ni ions from NiO nanoparticles increases

membrane permeability and ROS production causes cell death. Moreover antibacterial activity of Ni doped ZnO nanostructures electrostatic interactions between positively charged nickel ions and negatively charged cell membrane [45].

4. 4. Conclusion

Dye effluents from fabric industries have grown to be a serious environmental problem because of their unacceptable colour, high chemical oxygen demand and resistance to degradation. Zinc oxide nanostructures are a universal photocatalyst. We synthesized Ni doped ZnO nanoparticles via sonication method. The above synthesized samples proved to be more tremendous photocatalysts than ZnO by in contrast with until now reports. The doped ZnO nanoparticles show to be environment friendly materials for degrading contaminated colored waste water for reusing in cloth industry. Hence the synthesized doped nanoparticles prove to be higher marketers for environmental detoxing of organic compounds, detrimental dyes such as Rhodamine B, Rhodamine 60G, Methylene blue, and some metals too from waste water. Further antibacterial activity of tested against *E. coli* and *S. auerus* shows that Ni doped nanostructures possess better antibacterial effect due to the electrostatic interactions.

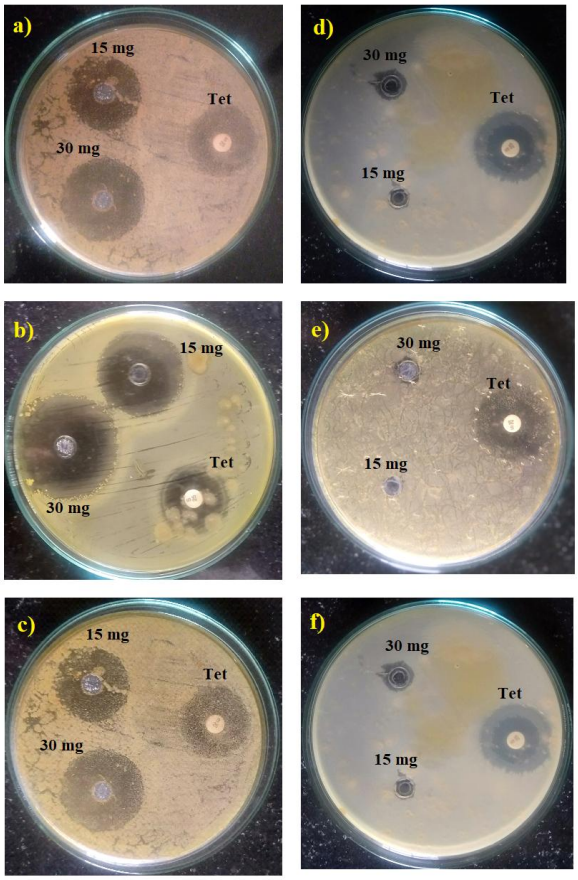

Fig. 7 shows Antibacterial activity of Ni doped ZnO nanostructures

References

1. Aleksandra Sosna-Głębska et al., (2019) Review on Metallic Oxide Nanoparticles sand Their Application in Optoelectronic Devices. Acta Innovations 2300-5599 30: 5-15 5
2. Su-Eon Jin et al., (2019) Photocatalytic antibacterial application of zinc oxide nanoparticles and self-assembled networks under dual UV irradiation for enhanced disinfe. International Journal of Nanomedicine 14:1737–1751
3. Anja Verbic et al., (2019) Zinc Oxide for Functional Textile Coatings: Recent Advances. Coatings 9:550 2- 26
4. Josue I. Garcia-Lopez et al., (2019) Foliar Application of Zinc Oxide Nanoparticles and Zinc Sulfate Boosts the Content of Bioactive Compounds in Habanero Peppers. Plants 8, 254 :3-20
5. Jinhuan Jiang et al., (2018) The Advancing of Zinc Oxide Nanoparticles for Biomedical Applications Bioinorganic Chemistry and Applications. 1062562:18
6. Baskaran Divya et al., (2018) Chemical Synthesis of Zinc Oxide Nanoparticles and Its Application of Dye Decolourization. Int. J. Nanosci. Nanotechnol., 14: 267-275
7. Yendry Regina Corrales Ureña et al., (2015) In situ sonochemical synthesis of ZnO particles embedded in a thermoplastic matrix for biomedical applications. Materials Science and Engineering C 49 : 58–65
8. Agnieszka Kołodziejczak-Radzimska et al., (2014) Zinc Oxide—From Synthesis to Application. A Review Materials 7:2833-2881
9. Varsha Srivastava et al., (2013) Synthesis, characterization and application of zinc oxide nanoparticles (n-ZnO) Ceramics International 39 9803–9808
10. V. Kavitha et al., (2019) Structural, optical and electrical studies on zinc doped barium strontium titanate as photo-anode for DSSC device (2019) Materials Today: Proceedings DOI: 10.1016/j.matpr.2019.05.437
11. V. Kavitha et al., (2019) Optical and structural properties of tungsten-doped barium strontium titanate, Materials Today: Proceedings, DOI: 10.1016/j.matpr.2019.05.351
12. Yin Zhang, Tapas R. Nayak, Hao Hong, and Weibo Cai (2013) Biomedical Applications of Zinc Oxide Nanomaterials. Curr Mol Med. 13(10): 1633–1645.
13. Dušan Nohavica et al., (2010) ZnO Nanoparticles And Their Applications – New Achievments . Nanocon 12- 14. 10. Olomouc, Czech Republic, EU
14. Pelangi Eka Yuwita et al., (2019) Structural, Optical, and Magnetic Properties of Mn-doped ZnO Nanoparticles Synthesized by Coprecipitation Method. Materials Science and Engineering 515 : 012065
15. U. Sachin Varma et al., (2018) Precipitation as a tool for Effective Doping of Magnesium in Zinc Oxide: Studies on Structural, Optical and Photocatalytic Properties.Rasayan. J.Chem. 11 4 :1491 – 1500
16. Gebretinsae Yeabyo Nigussie et al., (2018) Antibacterial Activity of Ag-Doped TiO_2 and Ag-Doped ZnO Nanoparticles. International Journal of Photoenergy 5927485: 1-7
17. D. Sathes Kumar et al., (2018) Violet Color Emitting Cd doped ZnO Nanoparticles for UV Sensor Applications. IJET. 4 2:904:908
18. Shakeel Ahmad Khan et al., (2017) Synthesis, characterization and evaluation of biological activities of

manganese-doped zinc oxide nanoparticles. TJPR 16 (10): 2331-2339
19. S.A.Khan et al., (2017) Comparative Synthesis, Characterization of Cu-Doped ZnO Nanoparticles and their Antioxidant, Antibacterial, Antifungal and Photocatalytic Dye Degradation Activities Digest Journal of Nanomaterials and Biostructures 12:3:. 877 – 889
20. Pricilla Jeyakumari et al., (2017) Structural, Optical and Antibacterial Activity of Pure and Cadmium Doped Zinc Oxide Nano Particles. IOSR-JAP. 2278-4861: 80-86
21. V.D. Mote et al., (2015) Structural, optical and antibacterial properties of yttrium doped ZnO nanoparticles Cerâmica 61: 457-461
22. Anh-Thu Thi Do et al., (2014) Effects of palladium on the optical and hydrogen sensing characteristics of Pd-doped ZnO nanoparticles. Beilstein J. Nanotechnol. 5: 1261–1267
23. B. Sankara Reddy et al., (2013) Physical and magnetic properties of (Co, Ag) doped ZnO nanoparticles J Mater Sci: Mater Electron 24:5204–5210.
24. Jagpreet Singh et al., (2019) Corrigendum to the effect of Manganese Doping on Structural, Optical, and Photocatalytic Activity of Zinc Oxide Nanoparticles. Composites Part B 165 :823
25. T.T. Nguyen et al., (2019) Preparation, Characterization and Photocatalytic Activity of La-Doped Zinc Oxide Nanoparticles. Materials 12 :1195
26. S. Senthil et al., (2018) Effect of chromium doping on structural, optical and photocatalytic properties of ZnO nanoparticles. Optoelectronics and Advanced Materials – Rapid Communications. 12 5-6:. 353 – 359
27. Siti Nur Aqilah Sulaiman et al., (2018) Effects of photocatalytic activity of metal and non-metal doped TiO_2 for Hydrogen production enhancement - A Review. IOP Conf. Series: Journal of Physics: 1027 012006
28. S. Ezhil Arasi et al., (2018) Effect of samarium (Sm^{3+}) doping on structural, optical properties and photocatalytic activity of titanium dioxide nanoparticles. Journal Of Taibah University For Science, 2: 186–190
29. K.C. Suresh et al., (2020) Evaluation of structural, optical and morphological properties of Nickel oxide nanoparticles for Multi-functional applications, Inorganic and Nano-Metal Chemistry DOI: 10.1080/24701556.2020.1770793
30. Cauê Ribeiro et al., (2017) The interplay between morphology and photocatalytic activity in ZnO and N-doped ZnO crystals Materials and Design 120 : 363–375
31. R.Jeyachitra et al., (2016) Effect of Ni doping on structural, optical and photocatalytic properties of $Zn_{1-X}Ni_XO$ nanoparticles prepared by different pH conditions, Journal of advance chemistry 12 6:4097-4107
32. Yang Wang et al., (2014) the Effects of Doping Copper and Mesoporous Structure on Photocatalytic Properties of TiO_2 Journal of Nanomaterials. 178152:1- 7
33. Anh-Thu Thi Do et al., (2014) High performance Ce-doped ZnO nanorods for sunlight-driven photocatalysis. Beilstein J. Nanotechnol. 4, 5: 1261–1267.
34. Dipti Vayaa et al., (2010) Study of synthesis and photocatalytic activities of Mo doped ZnO. Chem. Pharm. Res. 2(3):269-273
35. Kayode Adesina Adegoke et al., (2019) Synthesis, characterization and application of CdS/ZnO nanorods heterostructure for the photodegradation of Rhodamine B dye .Materials Science for Energy Technologies 2 :329–33
36. Adeel Riaz et al., (2019) Photocatalytic and Photostability Behavior of Ag and or Al-Doped ZnO Films in Methylene Blue and Rhodamine B Under UV-C Irradiation. Coatings 9: 202
37. Gaurav Hitkari et al., (2017) Synthesis, Characterization and Visible Light Degradation of Organic dye by Chemically Synthesized ZnO/γ-Fe_2O_3 Nanocomposites IJARSET4 5 :3960-3965
38. M. Sudha et al., (2020) Influence of synthesis methods on various properties of Zinc oxide nanostructures, The International journal of analytical and experimental model analysis, 12:1326-1338, DOI: 18.0002.IJAEMA.2020.V12I1.200001.015095
39. Patrícia Gonçalves et al., (2017) Evaluation of the Photocatalytic Potential of TiO_2 and ZnO Obtained by Different Wet Chemical Methods Materials Research 20 (2)n: 181-189
40. Karnaji et al., (2017) Photodegradation of Rhodamine B by using $ZnFe_2O_4$ Nanoparticles Synthesized through Precipitation Method. Materials Science and Engineering 202 : 012044
41. Ivan Mouritys Pereira Silvaa et al., (2016) Different dye degradation mechanisms for ZnO and ZnO doped with N (ZnO:N). Journal of Molecular Catalysis A: Chemical 417 : 89–100
42. Haiqing Yao et al., (2016) High-performance photocatalyst based on nanosized ZnO-reduced graphene oxide hybrid for removal of Rhodamine B under visible light Irradiation. AIMS Materials Science, 3(4): 1410-1425.
43. M. Sudha et al., (2019) Synthesis and Characterization of Lanthanum added ZnO Nanostructures, Journal of Information and Computational Science 9;12, 1548-7741 DOI:10.12733.JICS.2019.V9I12.535569.11243
44. K.C. Suresh et al., (2019) ZnO nanoparticles: Biosynthesis and characterization of its Multifunctional property Journal of Information and Computational Science 9:12, 1548-7741 DOI: DOI:10.12733.JICS.2019.V9I12.535569.11244
45. Balamurugan et al., (2019) 'Hydrothermal synthesis of samarium (Sm) doped cerium oxide (CeO_2) nanoparticles: Characterization and antibacterial activity', Materials Today: Proceedings, DOI: 10.1016/j.matpr.2019.08.217

